TELKOMNIKA, Vol. 11, No. 6, June 2013, pp. 2903 ~ 2911
e-ISSN: 2087-278X

Influencing Factors of Breaking Capacity of Double-Break Vacuum Circuit Breakers

Shengwen Shu*, Jiangjun Ruan, Daochun Huang, Gaobo Wu
School of Electrical Engineering, Wuhan University, Wuhan 430072, Hubei Province, China
*Corresponding author, e-mail: shushengwen@whu.edu.cn

Abstract

Using a series arrangement of two vacuum interrupters (VIs) has been proved to be an effective way of developing higher voltage vacuum circuit breakers (VCBs), which are known as double-break VCBs. The uniform distribution of the transient recovery voltage (TRV) across each VI is very critical for the breaking capacity of double-break VCBs. In this paper, the TRV distribution characteristics of double-break VCBs has been studied by the synthetic test and the PSCAD/EMTDC simulation based on a vacuum arc interruption model. The results show that the bias of the TRV distribution ratio is caused by the stray capacitance and the imbalanced post arc plasma characteristic in each VI, which is consistent with the theoretical analysis. Moreover, the negative effect of grading capacitors has been discussed. The results show that it is advisable to limit the value of grading capacitors to those ranges which can guarantee sufficiently improved voltage distribution.

Keywords*: VCB, double-break, breaking capacity, TRV distribution, grading capacitor*

1. Introduction

The vacuum circuit breaker (VCB) has been widely used in the low/medium voltage distribution system, while the SF_6 gas-blast circuit breaker (GCB) dominates the high/extra-high/ultra-high voltage circuit breakers fields [1-4]. Owing to the increasingly strict regulations in environmental protection, the SF_6 gas was specified as a kind of greenhouse gas in the Kyoto Protocol in 1997 and its emission has been strictly restricted [3-4]. Therefore, it is a trend to extend the application range of VCBs from low/medium to higher voltage levels.

The physical disadvantage of vacuum is the nonlinear relationship between dielectric strength and contact separation. The breakdown voltage is linear to a distance within about 10 mm. For greater contact distances, the saturation effect is evident [5]. This makes clear that so far the preferred range of the VCB is limited to the low/medium-voltage. Out of this reason it is a good idea to use a series arrangement of two or more vacuum interrupters (VIs) with short gap distances, which is known as double or multi-break VCBs. It is well known that in double and multi-break VCBs voltages appearing across each VI are not equal because of the stray capacitance. To keep the uniform distribution of the transient recovery voltage (TRV) across each VI is very critical for the successful breaking of double and multi-break VCBs. A usual method is to connect a grading capacitor with each VI.

Since the majority of VCBs in use are of the single-break variety, the characteristics of double and multi-break VCBs have not received sufficient attention. Nevertheless, there are still some useful research results concerning the TRV distribution ratio and influence of grading capacitors in the double and triple-break VCB. The TRV distribution ratio at the high voltage terminal in the double and triple-break VCB may reach up to 60% or higher [6-7]. In spite of connecting grading capacitors, the TRV distribution ratio after high current interruption may be uneven, and the results show that a bias of the TRV distribution ratio occurs when the post arc current value becomes imbalanced [3-4, 8]. Experimental results of a double-break VCB under different values of grading capacitors show that too large grading capacitance (>1500 pF) may be detrimental to the successful breaking [9]. When the VI at the high voltage terminal opens 2 ms later, grading capacitors reduce the breaking capacity of the double-break VCB instead [4].

But until now the TRV distribution mechanism of double and multi-break VCBs and the cause of the negative effect of grading capacitors have not been fully understood, which will be investigated in this paper taking the double-break VCB as an example. The paper is organized

Received January 9, 2013; Revised March 15, 2013; Accepted April 6, 2013

as follows. In section 2, the synthetic test circuit and parameters measuring method will be decribed, and a vacuum arc interruption model will be set up. In section 3, the experimental and simulation results will be provided and analyzed. Section 4 will conclude this paper.

2. Research Method

2.1. Synthetic Test Circuit

Figure 1 shows the experimental circuit of the measurement for the TRV distribution ratio in a double-break VCB, which is called the Weil-Dobke synthetic test circuit using current injection with the voltage circuit in parallel with the test circuit breaker. It consists of capacitor banks (C_{i1}-C_{i4}) and reactors (L_{i1}-L_{i4}) that are used as the current source and the capacitor bank (C_v) and reactor (L_v) that are used as the high voltage source.

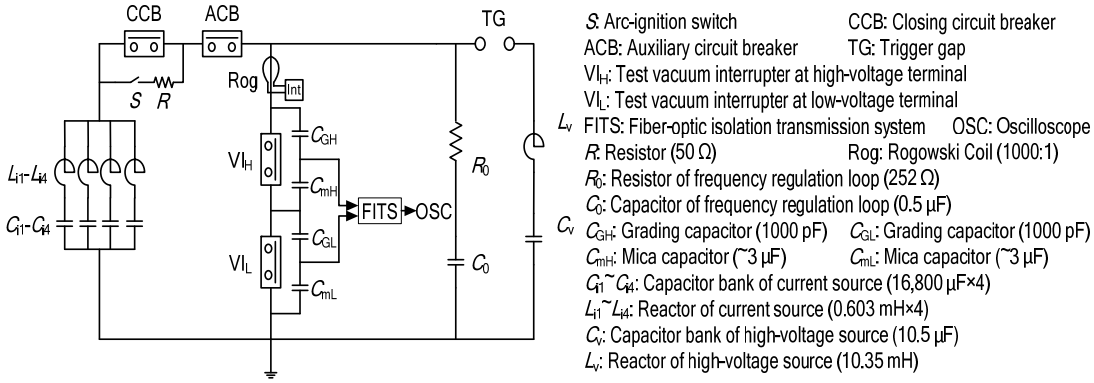

Figure 1. Synthetic Test Circuit of Measurement for TRV Distribution Ratio in a Double-Break VCB

Initially, the VI_2, VI_1 and the auxiliary circuit breaker (ACB) are closed; the CCB and the arc-ignition switch S are open. C_{i1}-C_{i4} and C_v are charged. Next, S is closed to supply an auxiliary current of tens of amps to the ACB and VIs. Immediately after the injection of this auxiliary current, the ACB is opened. After the gap length of ACB has reached its maximum value, CCB is closed to supply a main current of 50 Hz to VIs. Then, VIs are opened separately according to special requirements of the arcing time. At just before the zero point of the main current, the trigger gap (TG) is triggered, and then a current of 500 Hz but smaller amplitude derived from the voltage circuit is superimposed to the main current in VIs. Immediately after the interruption of the current in the ACB at the main current zero, the current source is separated from the voltage source and VIs are automatically connected into the voltage circuit. And immediately after the interruption of the superimposed current, the voltage supplied by the voltage source and adjusted by the frequency regulation loop (R_0 and C_0) is applied to VIs as the TRV, so there will be no delay between the current stress and the application of the voltage stress.

When measuring the TRV distribution ratio of the double-break VCB, the peak values of the interrupting current and TRV were set to about 17 kA and 60 kV respectively. Two test procedures were designed: the VI_H opens 0.5 ms and 2.5 ms later than the VI_L successively. A grading capacitor of 1000 pF was connected to each VI to eliminate the influence of the stray capacitance. With a method of adding a mica capacitor of 3 μF in series with the grading capacitor used, a capacitive voltage divider (VD) was formed automatically. The voltage signal was acquired by a voltage probe without attenuation and transmitted by a fiber-optic isolation transmission system (FITS) (ISOBE 5600), thus floating ground measurement for the TRV was realized. After that, the influence of the input capacitance of the VD on the TRV distribution ratio could be eliminated. Moreover, the current was measured by a Rogowski Coil and also transmitted by the FITS.

2.2. Vacuum Arc Interruption Model

Before simulating the influence of the post arc plasma characteristics on the TRV distribution ratio of double-break VCBs, it is necessary to establish a vacuum arc interruption model. In this paper, the VCB is represented with a black box model with changeable resistance rather than exploring the complex physical process of vacuum arc. The value of the resistance is altered to represent different phases during the current interruption process, which is mainly divided into arcing and post arc phases, as shown in Figure 2(a). Figure 2(b) illustrates the current zero phenomena of vacuum arc interruption. Figure 2(c) gives the structure of the black box model. Before a short circuit fault, the ideal switch S_1 is closed, the S_2, S_3 and S_4 are open, and hence the VCB displays the contact resistance R_{VI}. Once a fault occurs, the contact pair of the VCB opens, and then an arc forms. During the arcing phase the S_3 is closed, the S_1, S_2 and S_4 are open, so the VCB displays the arc resistance R_{arc}. During the post arc phase the S_1 and S_3 are open, the S_2 and S_4 are closed, so the VCB is represented by the post arc resistance R_{pa} in parallel with the gap capacitance C_{VI}. After the completion of the interruption, the S_4 is closed, the S_1, S_2 and S_3 are open, and hence the VCB displays the C_{VI}.

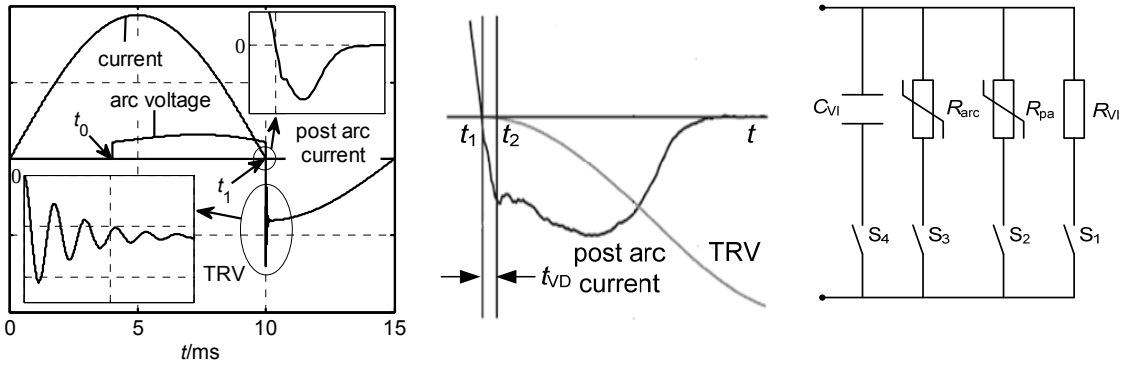

a) Whole Process of Vacuum arc Interruption

b) Current Zero Phenomena

c) Structure of Black Box Model of VCB

Figure 2. Vacuum arc Interruption Process and Model

During the arcing phase, the momentary value $u_{arc}(t)$ of the vacuum arc voltage in the diffuse mode can be written as [10]:

$$u_{arc}(t) = U_0 + r_0 v(t - t_0) i_{sc}(t) \quad t_0 < t < t_1 \tag{1}$$

where U_0 is the cathode voltage drop, r_0 is the assumed plasma resistance per meter gap length, v is the average opening speed, and v=1.5 m/s, $i_{sc}(t)$ is the momentary value of the short circuit current, t, t_0 and t_1 are the moments of arcing phase, opening of the contact pair and current zero, respectively.

Then the arc resistance can be calculated from the following equation:

$$R_{arc} = \frac{u_{arc}}{i_{sc}} \tag{2}$$

In order to determine the values of U_0 and r_0, the arc voltages under different currents for a commercial VCB with axial magnetic field (AMF) were measured, as shown in Figure 3.

From Figure 3, the arcing times were about 6.5 ms, and the RMS values of the arcing current were less than 20 kA. Because of the effect of the AMF, no constricted arcs appeared. In addition, the arc voltage and current had positive correlation. It can be obtained that U_0=16.35 V and r_0=0.06265 Ω/m by a linear fitting of the experimental data of the arc voltage and current in Figure 3.

For the post arc phase of vacuum arc interruption, the most widely used model is the "continuous transition model (CTM)" proposed by Andrews and Varey [11]. However, this model requires special treatment to make it numerically stable, which complicates its application [10]. When it is used for the double and multi-break VCB, this problem will become more prominent. Moreover, from Figure 2(b) it can be seen that a voltage zero phase immediately following current zero, i.e., the initial time of TRV (t_2) delays the moment of current zero (t_1) by a time period (t_{VD}). The CTM can not explain this phenomenon well.

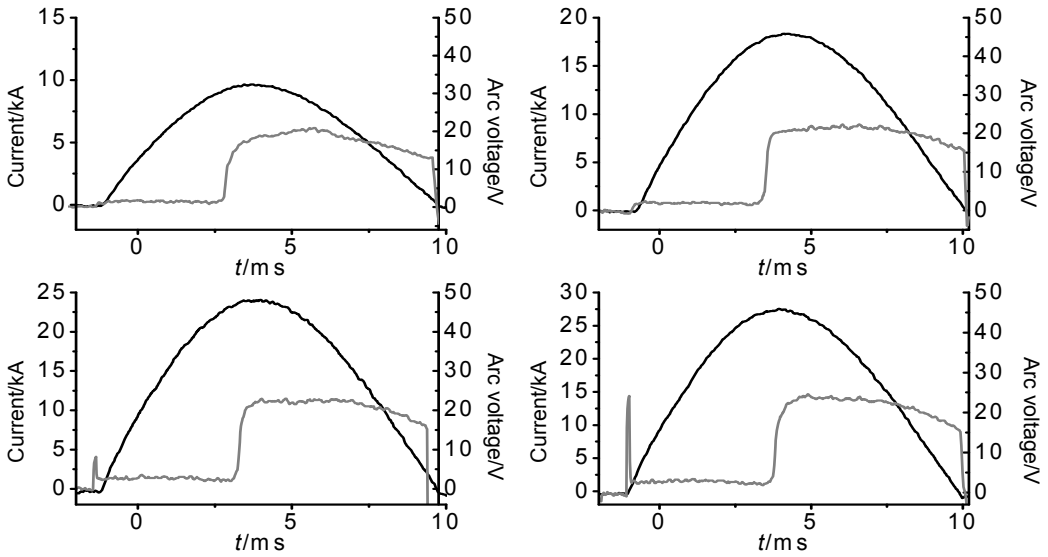

Figure 3. Measuring Waveforms of Arc Voltage and Current

The VCB's electrical behavior resembles that of a Langmuir probe [12]. By means of the plasma sheath, presheath and Bohm criterion in the theory of Langmuir probes, and taking the thermal velocity of the particles into account, the above voltage zero phase can be well explained. Therefore, the post arc current is modeled based on the theory of Langmuir probes, which is more stable and less complicated to implement. The model is represented by the following equations and implemented in the PSCAD/EMTDC,

$$i_{pa} = Z_i e N_i v_B A_{eff} \tanh\left(\frac{Z_i e u}{2kT_e}\right) + \frac{K}{u^{3/4}}\frac{du}{dt} \tag{3}$$

$$A_{eff} = A + c_1 u \tag{4}$$

$$\frac{dN_i}{dt} = -\frac{N_i}{\tau} - \frac{i_{pa}}{Z_i e c_2} \tag{5}$$

$$v_B = \sqrt{\frac{kT_e}{m_i}} \tag{6}$$

$$K = 0.42 A_{eff} \left(Z_i e N_i \varepsilon_0\right)^{1/2} \left(\frac{kT_e}{Z_i e}\right)^{1/4} \tag{7}$$

where i_{pa} is the post arc current, Z_i is the average ion charge, e is the elementary charge, N_i is the ion density, k is the Boltzmann's constant, T_e is the electron temperature, m_i is the ion mass,

A_{eff} is the effective cathode area, A is the contact's surface area, u is the voltage across the VCB, c_1 is a constant which reflects that the A_{eff} increases linearly with the voltage, τ is the time constant for the natural decay, c_2 is a constant which relates the post arc current to the ion density decay, v_B is the Bohm velocity, and ε_0 is the permittivity in vacuum.

Hence the post arc resistance can be calculated from the following equation:

$$R_{pa} = \frac{u}{i_{pa}} \tag{8}$$

Because t_{VD}<<τ, at t=t_2 in Figure 2(b),the N_i can be assumed to maintain its initial value N_{i0}, and the post arc current only consists of the ion saturation current, which can be calculated as follow:

$$i_{i,sat} = Z_i e N_{i0} v_B A \tag{9}$$

On the other hand, during the time period t_1~t_2, the current ramp di/dt can be approximately considered as a constant, which is the same as di/dt at t=t_1, thus

$$i_{i,sat} = di/dt|_{t=t_1} \cdot t_{VD} \tag{10}$$

Equations (9) and (10) connect the arcing phase with post arc phases.

The quantities Te, mi, Zi, and τ cannot be measured with our equipment and their value have to be estimated or taken from the literatures [12]-[14]. It is assumed for the simulation that Te, mi, and Zi are 3 eV, 1.06×10-25 kg and 1.85 (constant), respectively, and the values of τ, c1 and c2 are adjusted to make the simulation approach experiment.

Table 1. Values of c_1 Under Different Rising Rates of TRV

Rising rate of TRV (kV/μs)	15	6	4
Value of c_1(m^2/V)	2×10^{-6}	1×10^{-6}	5×10^{-5}

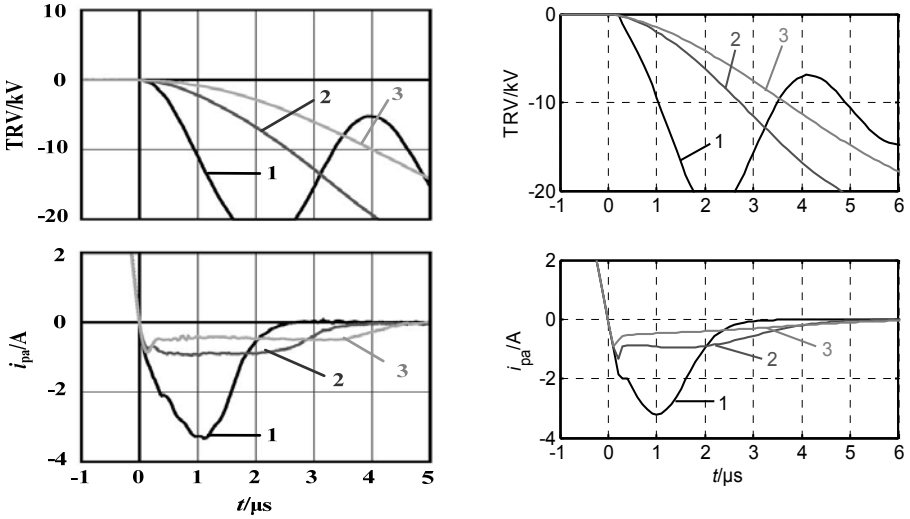

(a) Measured Waveforms (b) Simulation Waveforms

Figure 4. TRV and Post-arc Current Under Different Rising Rates of TRV

Figure 4(a) illustrates the measured waveforms of the TRV and post arc current under different rising rates of TRV, and corresponding simulation waveforms are shown in Figure 4(b). Because the three measurements were performed with equal settings, it should be expected

that the initial plasma conditions were equal as well. As a consequence, the model's parameters should be the same in all three simulations. The parameters Ni0, τ and c2 remained indeed unchanged (7×1017 m-3, 5 μs and 3.3×10-5 m3, respectively), but only c1 had to be adjusted to match the measured waveforms, as shown in Table 1. Therefore, the assumed relation between the effective cathode area and the voltage in Equation (4) is inadequate and needs to be improved.

It can be seen from Figure 4 that the simulation waveforms are practically identical to the measured waveforms after selecting appropriate parameters. The difference between the simulation and measured post arc current is noticeable only in the short interval before it declines to zero. Therefore, the described model has been proved to be accurate enough to be used to the simulation of double-break VCB in the next section.

3. Results and Analysis

3.1. Experimental Results

Figures 5(a) and (b) show the measured waveforms of the TRV in a double-break VCB when the VI_H opens at 3.5 ms while the VI_L opens at 3 ms, and the VI_H opens at 1.3 ms while the VI_L opens at 3.8 ms, respectively.

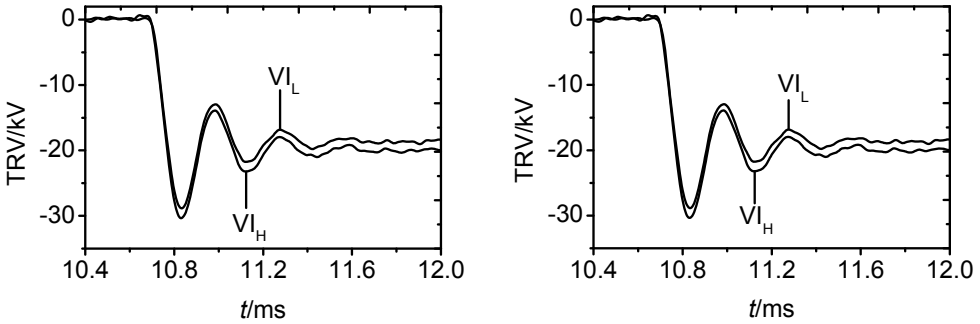

(a) VI_H opens 0.5 ms later than the VI_L (b) VI_H opens 2.5 ms later than the VI_L

Figure 5. Measured Waveforms of TRV in a Double-Break VCB

From Figure 5, the voltage distribution ratios at the TRV crest in the two test procedures are VI_H: VI_L=51.0%: 49.0% and VI_H: VI_L=51.3%: 48.7%, respectively. So it can be concluded that the delayed opening of the VI_H may lead to a more uneven TRV distribution in the double-break VCB.

3.2. Simulation Results

The transient equivalent circuit of double-break VCBs for simulation can be represented as shown in Figure 6. According to the measured results, it is assumed that C_H=C_L=19 pF and C_S=28 pF. The R_{paH} and R_{paL} are calculated by the vacuum arc interruption model described in Section 2.2.

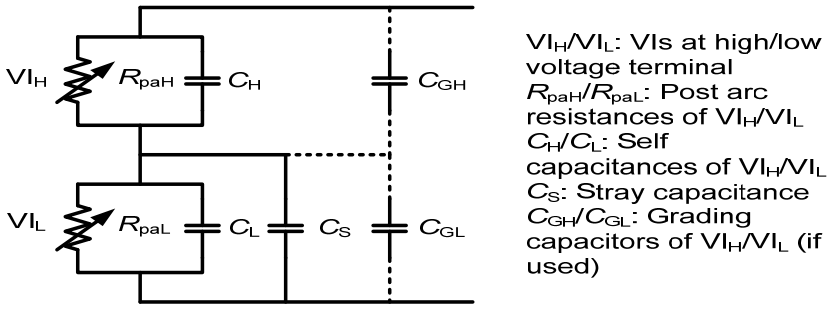

Figure 6. Transient Equivalent Circuit of Double-Break VCBs

Three simulation procedures were designed to obtain different TRV distribution ratios in the double-break VCB by changing some parameters in the vacuum arc interruption model, which are specified on Table 2. And Figure 7 gives the simulation waveform of procedure 3 as a typical example.

Table 2. Simulaiton Parameters and Results

No.	Break	Parameter N_{i0}(m^{-3})	Parameter τ(μs)	Grading capacitor	Result
1	VI_H	2×10^{18}	4	without	69.9%
	VI_L	2×10^{18}	4		30.1%
2	VI_H	1×10^{18}	2		82.3%
	VI_L	2×10^{18}	4		17.7%
3	VI_H	1×10^{18}	2	200 pF	63.6%
	VI_L	2×10^{18}	4		36.4%

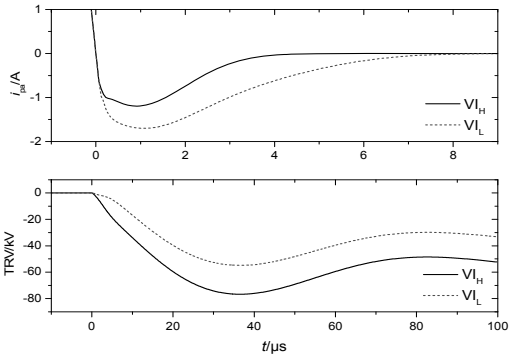

Figure 7. Simulation Waveform of Procedure 3

In procedure 1, the plasma parameters of the VI_H and VI_L are the same, so the bias of the TRV distribution ratio is only caused by the stray capacitance. In procedure 2, the initial ion density in the VI_H is less and decays more quickly than that in the VI_L. This results in a more uneven TRV distribution ratio than procedure 1. In procedure 3, in spite of connecting a grading capacitor of 200 pF with each VI, the TRV distribution ratio is still very unbalanced because of the difference of the ion density between the VI_H and VI_L.

3.3. Analysis of TRV Distribution Mechanism of Double-Break VCBs

According the experimental and simulation results listed in Section 3.1 and 3.2, it can be concluded that the bias of the TRV distribution ratio in double-break VCBs may also be caused by the imbalanced post arc plasma characteristic in each VI besides the stray capacitance. Using circuit principles in Figure 6, the bias of the TRV distribution ratio can be calculated as follow:

$$\begin{cases} \Delta U = \dfrac{\int_0^t i_{(C_H+C_{GH})}\mathrm{d}t}{C_H+C_{GH}} - \dfrac{\int_0^t i_{(C_L+C_S+C_{GL})}\mathrm{d}t}{C_L+C_S+C_{GL}} \\ i_{(C_H+C_{GH})} - i_{(C_L+C_S+C_{GL})} = i_{paL} - i_{paH} \end{cases} \tag{11}$$

where i_{paH} and i_{paL} are the post arc currents flowing through the VI_H and VI_L, respectively.

If grading capacitance is much greater than the self and stray capacitance, Equation (11) can be simplified as:

$$\Delta U = \frac{\int_0^t (i_{paL} - i_{paH})\mathrm{d}t}{C_G} \tag{12}$$

It can be seen from Equation (12) that in spite of connecting grading capacitors, the TRV distribution ratio may be uneven because of the difference of the post arc currents, as the simulation result shown in Figure 7. The analysis of the experimental results is similar. When the VI_H opens later than the VI_L, the initial ion density in the VI_H is lower, and this is similar to the situation of the simulation procedure 3. Nevertheless, the difference between the two test procedures is not obvious, because the interrupting current is not high enough to generate a high post arc current and the value of grading capacitor is a bit large.

3.4. Cause Analysis of Negative Effect of Grading Capacitors

In double-break VCBs, the VI_H usually reignites first because it takes over most of the TRV as a result of the stray capacitance. When the rising rate of the TRV is below a certain threshold, the breakdown of the VI_H doesn't lead to a failure of the whole arrangement, because the dielectric strength of the VI_L may exceed the TRV and is able to take over the whole TRV for a moment. Once the VI_H is recovered, the VI_H and VI_L will complete the interruption together. This explains the improvement of the breaking behavior of the double arrangement compared with a single interrupter.

Figure 8 shows the dependence of the amplitude of re-ignition current of the re-ignition voltage and grading capacitance obtained by calculation, simulation and test. Figure 9 gives the dependence of the duration of the re-ignition current of the grading capacitance [15].

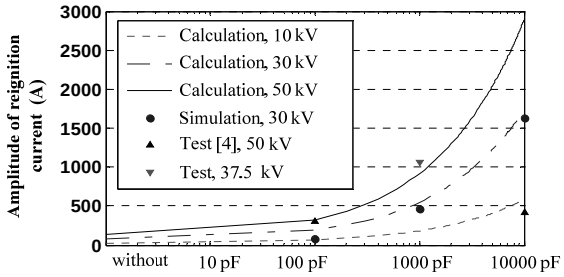

Figure 8. Amplitude of Reignition Current vs Reignition Voltage and Grading Capacitance

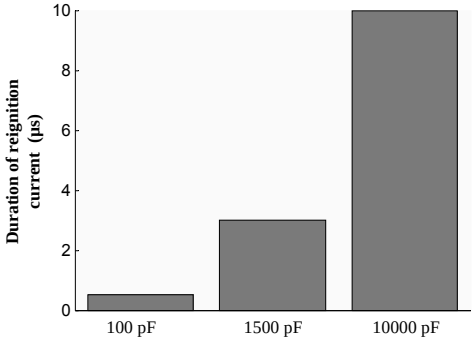

Figure 9. Duration of Reignition Current vs Grading Capacitance

From Figures 8 and 9, the amplitude and duration of the reignition current significantly increase with the values of grading capacitors. As a result, the energy exporting into the contact gap increases and is enough to melt some mm^3 of the contact material [11]. From this a local strong heating of the contacts seems to be possible which may be a source of generation of additional metallic carriers into the contact gap and as a result the series arrangement fails. Furthermore, the interrupter without reignition has to take over the whole TRV for a much longer time. These above-mentioned two aspects may explain the finding that with higher values of the grading capacitors no further improvement of the breaking capability can be achieved.

4. Conclusion

This paper studies the TRV distribution characteristics of double-break VCBs by means of the synthetic test and the PSCAD/EMTDC simulation based on a vacuum arc interruption model. The results reveal that the bias of the TRV distribution ratio is caused by the stray capacitance and the imbalanced post-arc current as a result of the difference of the post arc plasma characteristic in each VI. Furthermore, too large grading capacitance may lead to a decrease of the breaking capacity of double-break VCBs. Thus, it is advisable to limit the value of the grading capacitors in such a range to sufficiently improve the TRV distribution in double-break VCBs.

Acknowledgements

This paper is supported by the National Eleventh-five Year Science and Technology Supporting Program of China (2009BAA19B05).

References

[1] Dong EY, Yin GX, Wang YX, Duan XY, Zou JY. The application of NdFeB in the magnetic force actuator. *TELKOMNIKA*. 2012; 10(6): 395-1402.

[2] Haryono T, Tunggul SK, Tumiran, Berahim H. The damage of ZnO arrester block due to multiple impulse currents. *TELKOMNIKA*. 2011; 9(1): 171-182.
[3] Shiba Y, Ide N, Ichikawa H, Matsui Y, Sakaki M, Yanabu S. Withstand voltage characteristics of two series vacuum interrupters. *IEEE Transactions on Plasma Science*. 2007; 35(4): 879–884.
[4] Ide N, Tanaka O, Yanabu S, Kaneko S, Okabe S, Matsui Y. Interruption characteristics of double-break vacuum circuit breakers. *IEEE Transactions on Dialectical Electrical Insulation*. 2008; 15(4): 1065–1072.
[5] Giere S, Karner HC, Knobloch H. Dielectric strength of double and single-break vacuum interrupters. *IEEE Transactions on Dialectical Electrical Insulation*. 2001; 8(1): 43–47.
[6] Betz T, Konig D. Influence of grading capacitors on the breaking capacity of two vacuum interrupters in series. *IEEE Transactions on Dielectrics and Electrical Insulation*. 1999; 6(4): 405-409.
[7] Huang DC, Ruan JJ, Wu GB, Xu J, Shu W, Zhang K. Potential and electric field distributions of modular multi-break vacuum circuit breaker. *High Voltage Engineering*. 2012; 37(1): 124-130.
[8] Sugita M, Igarashi T, Kasuya H, Okabe S, Matsui Y, Lanen E, Yanabu S. Relationship between the voltage distribution ratio and the post arc current in double-break vacuum circuit breakers. *IEEE Transactions on Plasma Science*. 2009; 37(8): 1438–1445.
[9] Fugel T, Koening D. Influence of grading capacitors on the breaking performance of a 24-kV vacuum breaker series design. *IEEE Transactions on Dielectric and Electrical Insulation*. 2003; 10(4): 569-575.
[10] Martin BJ. Vacuum interrupter model based on breaking tests. *IEEE Transactions on Plasma Science*. 1999; 27(4): 969-976.
[11] Andrews JG, Varey RH. Sheath growth in a low pressure plasma. *Physics of Fluids*. 1971; 14(2): 339-343.
[12] Lanen EPA, Smeets RPP, Popov M, Sluis L. Vacuum circuit breaker postarc current modeling based on the theory of Langmuir probes. *IEEE Transactions on Plasma Science*. 2007; 35(4): 925-931.
[13] Johannes K. Measurements and modeling in the current zero region of vacuum circuit breakers for high current interruption. *IEEE Transactions on Plasma Science*. 1997; 25(4): 632-636.
[14] Gilles R, Weltmann KD, Schade E, Claessens M. Numerical simulation of residual charge of vacuum interrupters. *IEEE Transactions on Plasma Science*. 2001; 29(5): 754-758.
[15] Betz T, Konig D. *Switching and transient phenomena in a series design of two vacuum circuit breakers*. International Symposium on Discharges and Electrical Insulation in Vacuum. Yalta, Ukraine. 2004; 2: 399-402.